Hindawi
Advances in Materials Science and Engineering
Volume 2022, Article ID 8319044, 18 pages
https://doi.org/10.1155/2022/8319044

Research Article

Hysteresis Behavior and Design of the New Autoclaved Lightweight Concrete (ALC) External Panel Connector with the Steel Frame

Kewei Ding,[1] **Chikun Zhang**,[1,2] **Shulin He**,[1] **and Yunlin Liu**[1]

[1]*College of Civil Engineering, Anhui Jianzhu University, Hefei, Anhui 230601, China*
[2]*Architecture and Civil Engineering, City University of Hong Kong, Kowloon Tong 999077, Hong Kong*

Correspondence should be addressed to Kewei Ding; dingkw@ahjzu.edu.cn

Received 18 November 2021; Revised 22 January 2022; Accepted 25 January 2022; Published 22 February 2022

Academic Editor: Rotana Hay

This paper proposes a new flexible connector for the autoclaved lightweight concrete (ALC) panel with the steel beam. It is a universal upper and lower crossing connector, with load-bearing and limitation holes; then, the seismic capacity of this connector is investigated in the simulations and full-scale tests. Firstly, the finite element simulations of the new connector and traditional connector (L-hooked bolt) were made by ABAQUS, which proved the reliability of the new connector by comparing them in low-cyclic loading. Secondly, in order to analyze the phenomenon and data of the two connectors which are in the same test conditions of simulation, the full-scale tests of the steel frame were conducted. The damage of the ALC panel at different connectors and at different test load displacements is described in detail. The contribution of the connectors to the steel frame and the ALC panel is investigated in depth during the elastic, elastoplastic, and plastic stages of the steel frames. The test result is similar to the simulation result roughly, in which the new connector has better seismic capability. In minor earthquakes, the ALC panel frame with the new connector has better synergistic capacity of panels, while in large earthquakes, it can provide certain stiffness to the structure. Compared with the L-hooked bolt, the maximum bearing capacity of the structure with the new connector increases by 5.2%, and the yield displacement delays by 27.5%, which results in the increase of ductility by 9.8%. In terms of energy consumption capacity, the equivalent damping factor of the new connector increases by 10.2% and 35.3% at the yield and ultimate state, respectively. The FEM simulation results can represent the actual test results well. To summarize, the new ALC panel connector in this paper has excellent seismic capacity and good synergistic, which can provide a reference for the development and application of new types of the ALC connector.

1. Introduction

Along with rising housing demand as a result of growing urbanization, prefabricated building is thought to be a cost-effective and environment-friendly way to address this problem [1–3]. Steel structure is currently one of the main choices for the development of prefabricated buildings, and the enclosure system is a critical component of the prefabricated structure, and its capabilities have a direct impact on the building's overall capacity [4]. In prefabricated steel structures, autoclaved lightweight concrete (ALC) has been proposed for application in building enclosure systems. ALC allows for a reasonable reduction in enclosure weight due to the prefabricated system's light self-weight, as well as an increase in assembly and transportation efficiency [5]. ALC panel is a new type of panel that merges lightweight panel technology and concrete block technology, which is formed by high temperature, high pressure, and steam curing using a specific technique [6]. In nonstructural applications, although the recycled aggregate concrete (RAC) has better compressive strength [7], the ALC meets specifications and has higher productivity [8]. In comparison to typical solid clay bricks and hollow clay bricks, ALC panels have a low gravity and resistance of fire and seepage, which provide superior construction physical capacity. Although double-skin façade (DSF) and AAC block panels can have these

advantages better, they are not as easy to construct as ALC panels [9–11]. Currently, research on ALC panels is mostly focused on the improvement of the stiffness, seismic resistance, and energy consumption of the whole building structure [12]. In terms of simulation, Qu et al. [13] conducted structural testing and numerical modeling on four ALC panels, and the test panel was simulated using finite element software. By using numerical modeling, Matteis and Landolfo [14] researched the seismic reaction and assessed the hysteretic capacity and energy dissipation capacity of a steel frame structure wrapped in the light wall panel. In terms of test, Yang et al. [15] investigated the hysteresis capacity of the hinged steel frames with embedded ALC panels and found that the hysteresis capacity of the panels connected by the tube connector is better than the U-connector, although both of them have good synergistic capacity. Wang et al. [16] studied repeated low-cycle loading tests on ALC panels and block-filled CFST frame structures in order to determine the effect of U-shaped steel clips, L-hooked bolts, swinging connectors, and angle steel on the seismic capacity of panels. For determining the displacement ductility of ALC panels, Zhang et al. [17] conducted four-point loading experiments on six ALC external panels and three roof panels. Gou et al. [18] expounded the construction process, installation and operation points, material and equipment input, the quality control, and other aspects of the ALC panel, according to engineering examples on-site. Among the prefabricated ALC panel building structures, cladding and embedding are the most common connectors between prefabricated external wall panels and the main structure [19]. Not only should the structure be securely connected when the panel and frame cladding connector are used but the deformation of the two components should also be coordinated under a variety of impacts [20]. If the connector is damaged during an earthquake, the panel would collapse which means it would cause secondary accidents [21]. There are few studies on the connector of cladding panels in China, and the most commonly used connector is the L-hooked bolt on-site. Although the L-hooked bolt has a high bearing capacity when the structure is in obvious displacement, it would crack especially in mortar joints just under slight seismic load, which would make the whole structure of heat insulation and thermal insulation drop drastically [22, 23].

Based on these achievements, a NALC connector, which requires secondary special cement pouring, was invented and used in its own research of NALC panel by Nanjing Xujian Company [24]. This type of connector could increase the time of wet work and reduce the efficiency of assembly work because it needs to be poured twice on-site. In order to improve the external ALC panel connector, Cao et al. [25] developed an embedded ALC connector that consists of embedded components, stiffening plate, and steel angle. Although the embedded connector partially solves for the L-hooked bolt connector problem, its construction is complicated and expensive. ALC panels require high-temperature and high-pressure manufacturing, which can deflect or deform the preburied parts so that they could not set up on-site. In addition, transportation may also cause damage to the embedded ALC panels [26, 27]. Bai proposed a flexible ALC panel connector, while the connector is much complicated because it is divided into different shapes of above and below [28].

To solve these problems, a new connector was proposed based on previous works, named crossing ALC panel connector. Instead of being hooked by a traditional L-hooked bolt, the ALC panel is supported from the bottom by a new connector. Additionally, the limitation hole is designed to resisting seismic loads which can achieve a flexible connector of panels, steel beams, and columns. The limitation hole can also increase the part of freedom during installation. This connector has the following advantages: beyond wet work, simple design, quick assembling, and great seismic capacity. To ensure the connector's reliability, the simulations and low-cyclic reversed load tests were taken by using ABAQUS and full-scale steel of low-cyclic reversed load, respectively. According to the investigation, the new crossing connector offers a comprehensive range of functions, which could replace the traditional L-hooked bolt for steel constructions.

The remainder of this paper is organized as follows: in Section 2, the design details of the new connector, the conditions for building the finite element model, and the simulation results are presented. Section 3 introduces the test details including the assembling process, material properties' test, test device, and loading system. Section 4 provides the test results including the detailed phenomenon and the hysteresis curves of each specimen. As for Section 5, the seismic capacity of the new connector and traditional L-hooked bolt is analyzed in depth. Finally, Section 6 summarizes and concludes the content of the full work.

2. Design and Simulation

2.1. Connector Design. When the building structure undergoes a significant lateral shift, the damage of the ALC panel can be decreased proportionally to its sway caused by the connector. As a result, a new connector was designed to interconnect the ALC panel and steel frame, named the crossing ALC panel connector. The new integral structural system can be coordinated well in response to resisting or dissipating external forces by connector deformation (internal displacement of bolts) and maintain the stability and integrity of the whole wall system. It can ensure that the whole wall does not crack under high-frequency low-level earthquakes (small interstory displacement deformation). It can also provide certain stiffness to the structure in the large earthquake. This can also increase the part of freedom during assembling and can avoid some problems that cannot be set up due to inconsistent accuracy and transportation collisions. This connector with good aseismatic behavior can easily achieve the antiseismic design principles, named "strong joint-weak member." [29]

The new crossing ALC panel connector is a cross-shaped connector composed of load-bearing and restriction holes. It consists of the following components: I-beam, ALC panel, cross-shaped connector, bolt, and nut. To facilitate installation, a slotted hole is opened in the upper part of the

connector to serve the lower load-bearing node for the upper exterior wall panel, bearing the vertical, outward horizontal, and inward horizontal loads of the upper exterior wall panel; a long circular hole is opened in the lower part of the connector in the horizontal direction (limitation hole), with a hole diameter slightly larger than the diameter of the bolt; the type of upper bolt hole is long circle. Both upper and lower connectors can bear the weight and limit the slip, but the lower node completely limits the slip in the horizontal direction. It is possible for the panel and the central structure to generate followership. The ALC panel connector is shown in Figure 1.

2.2. Finite Element Analysis Models. ABAQUS finite element analysis software was used to analyze the capacity of the new connector by comparing with the traditional L-hooked bolt [30]. The length of the L-hooked bolt was 200 mm, and the specification was M12. Q235 and Q345 grade hot-rolled H-beams were selected. The steel beam length was 3800 mm, and its size was HM 244 mm × 175 mm × 7 mm × 11 mm. Steel column height was 3888 mm; its size was HW 200 mm × 200 mm × 8 mm × 12 mm. The dimensions of the ALC panel were 3000 mm × 600 mm × 200 mm. Two models are exhibited in Figure 2 consisting of five ALC panels with five sets of traditional L-hooked bolt and new panel connector, respectively.

The ALC, connector, and steel beam used C3D8R hexahedral linear reduction integral solid elements, and the reinforcement used T3D2 linear truss elements [31, 32]. The grids at the connectors and hole of the ALC panel were refined, while the rest of the grids were sparse. The ALC panel was made of ALC and reinforcement which used the plastic damage model. The connector used Q345B, and the steel beam and column used Q235B [33]. A3.5B05 standard was chosen for the ALC panel. An elastoplastic constitutive model of ALC panel was used according to previous studies [34, 35], shown in Figure 3.

All welding processes were replaced by the "Tie" constraint (between beams and columns, between connectors and beams, etc.). By considering the relationship between reinforcement and concrete, the embed command (built-in command) was used to embed the reinforcement directly into ALC panels [36]. Because ALC is only about 1/8–1/10 of the strength of ordinary concrete, it is easy to crush and make the friction effect smaller. Therefore, the principle that the maximum static friction coefficient and sliding friction coefficient are approximately equal is adopted. To simulate real contact, the method of defining friction coefficients by tangential characteristics is used. The contact surfaces between the connectors, bolt, and panel were set to hard contact. The friction coefficient μ_1 between the connector and ALC panel is taken as 0.2, and the friction coefficient μ_2 between the panel and panel of ALC is taken as 0.3 [37].

The coupling point was constrained and loaded in accordance with the boundary conditions of some research studies, which included displacement constraints in the x- and z-directions ($u_y = u_z = 0$) and rotation constraints in the x- and z-directions ($x = y = z = 0$) on the top of the column, as well as rotation constraints in the x- and z-directions ($x = y = z = 0$) on the bottom of the column. In addition to the displacement restriction at the bottom of the column ($u_x = u_y = u_z = 0$), it was a rotation constraint in the x- and z-directions ($x = y = z = 0$). The pretightening force for the 10 connector bolts was determined by 1 kN bolt pretension force. A vertical axial compressive force was imposed at the opposite side of the contact surface between the steel column and beam. This force was cyclic load which was applied at the coupling point, shown in Figure 4. The load was controlled by the displacement angle, where the maximum displacement was 130 mm. Three turns were loaded at each stage before 30 mm, and two turns were loaded at each stage afterwards (since 40 mm stage) [38].

2.3. Result of the Finite Element Simulation. According to the simulation results, it can be seen that the two connectors have a similar trend under displacement loading (±135 mm maximum), both experiencing elastic and yielding stages. From force-displacement hysteric curves (Figure 5(a)), the hysteresis loop of the new connector (FEM2) covered the hysteresis loop of the L-hooked bolt (FEM1), indicating that the energy dissipation capacity of new connectors was better. Meanwhile, the new connector (169.95 kN) has the better load capacity than the L-hooked bolt (189.33 kN) according to the skeleton curves (Figure 5(b)) which increases by 11.4% averagely. To further confirm the function of the new connector, full-sized tests are necessary.

3. Details of Test Research

3.1. Test Design. Full-sized steel frames were used for the low-cyclic reversed load test. According to the standard of residential building height, column span, beam, and column section size, the final design is a single span flat steel frame which is 3888mm storey height and 3800mm storey width, which was the same as the size and material of finite element analysis models in Section 2. The wall was made of 5 external ALC panels, and the seams of the panels were made of ALC panels' special patchwork binder. All specimens are prefabricated at the factory according to dimensional requirements. In this test, there are two sets of specimens to connect the panel and the main frame, respectively, and specimens are shown in Figure 6.

After all the specimens were produced and maintained, they were delivered and assembled on the test site. The setup process and overview of test specimens are shown in Figures 7 and 8.

3.2. Test Facility and Setup. The test utilizes an American MTS servo loading system with a 500 mm actuator displacement stroke. A quasi-static loading strategy was used in this test: a horizontal low-cycle reciprocating load was given to the column's top panel, and the column's top panel was coupled to the hydraulic servo actuator. Figure 9 illustrates the test facility.

As shown in Figure 10, the test loading device includes an electrohydraulic servo loading system, hydraulic jack, hydraulic actuator, connecting rod, anchor bolt, and

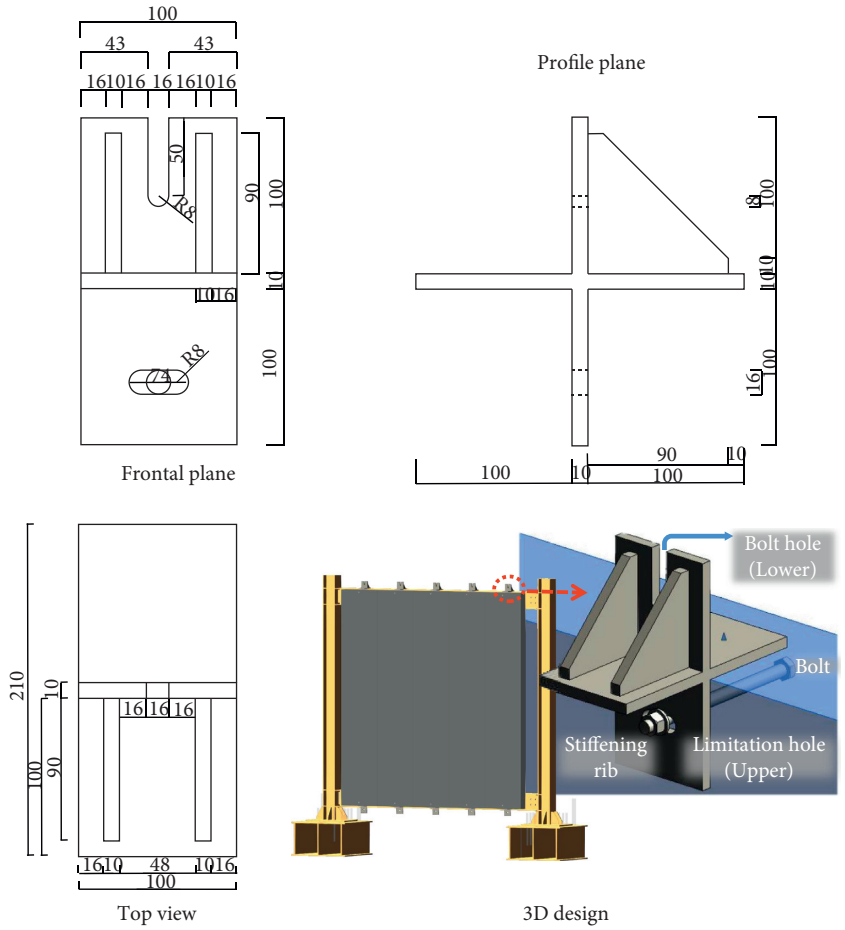

Figure 1: Geometric dimension of the new connector.

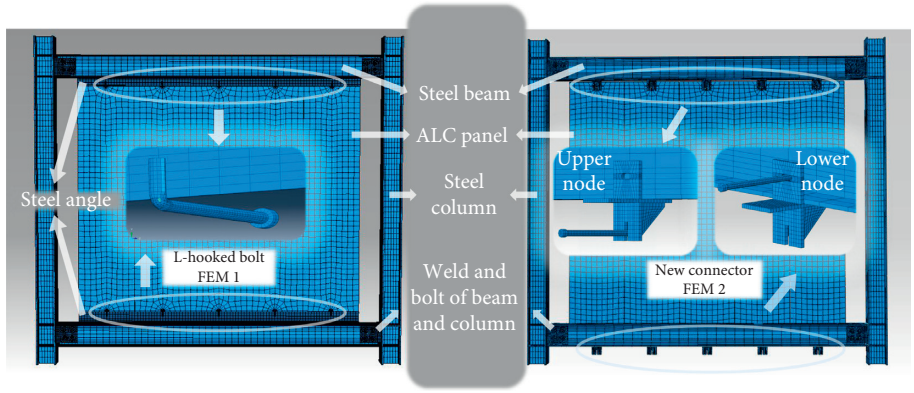

Figure 2: Finite element analysis models.

reaction frame. The electrohydraulic servo loading system is attached to the actuator for the loading test.

3.3. Material Properties. Six ALC cube test blocks measured 100 mm × 100 mm × 100 mm and three ALC rectangular test blocks measured 100 mm × 100 mm × 300 mm [39] were poured under the same conditions as stated in Figure 11. Steel coupons were cut from steel tubes and sheets and tested for tensile strength, modulus of elasticity, and breaking elongation by using the universal testing machine, as shown in Figure 12. The result of steel material tests is summarized in Table 1, and the mechanical ALC panel is shown in Table 2, which shows few differences of material properties of the test and simulation.

3.4. Loading System of the Test. The loading protocol for the tests is FEMA 461 [40], in which the displacement-controlled method was employed for 0.5 mm/s low rate loading.

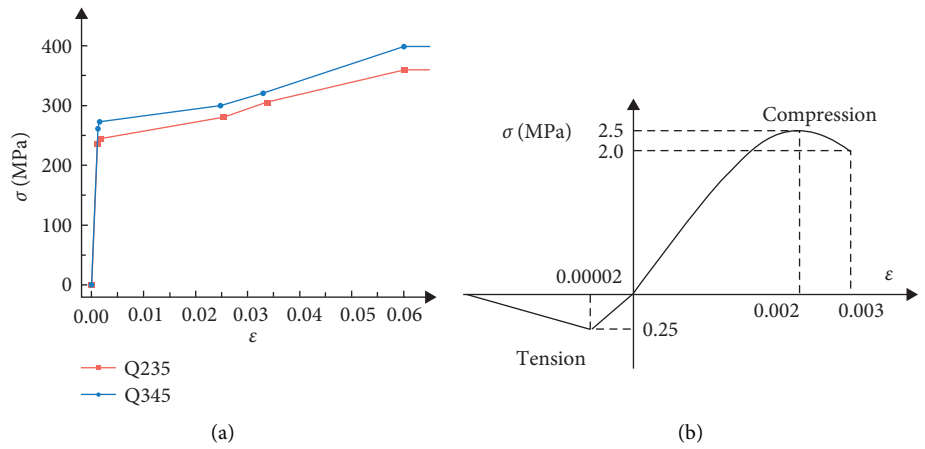

Figure 3: Stress-strain curves of the materials. (a) Constitutive curve of steel. (b) Constitutive curve of the ALC panel.

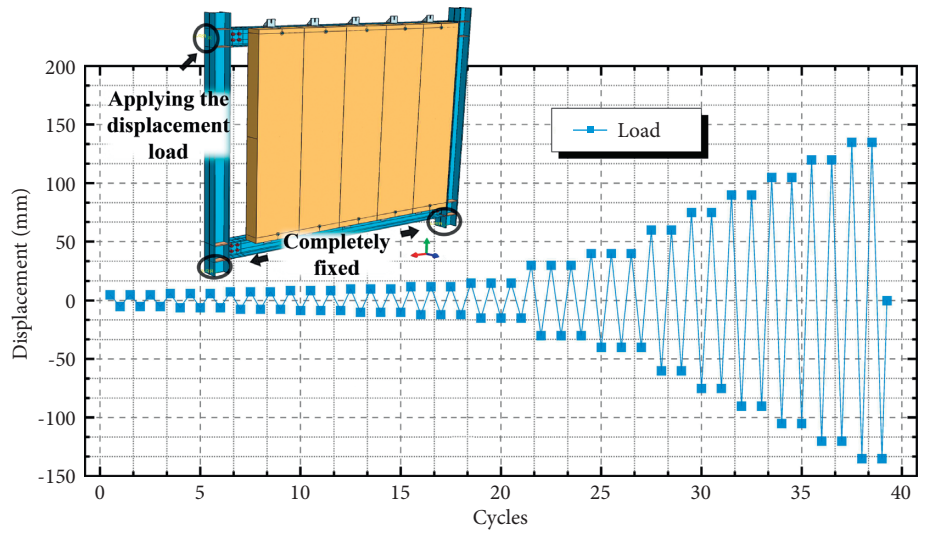

Figure 4: Boundary and loading system.

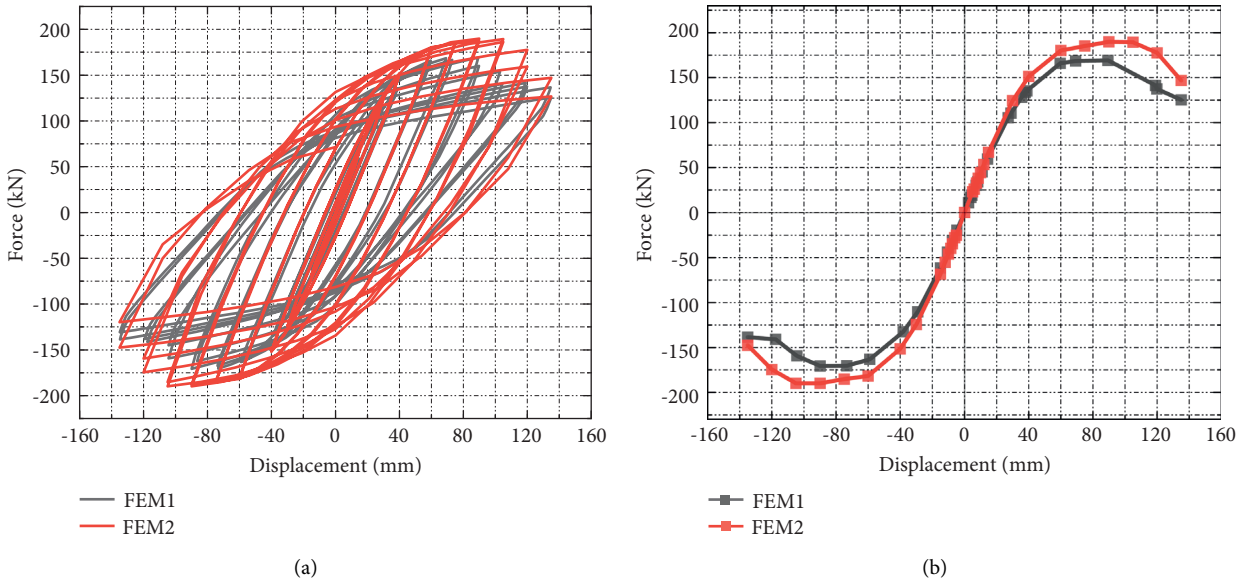

Figure 5: Simulated comparison. (a) Load (force)-displacement hysteric curves. (b) Skeleton curves.

(a) (b)

Figure 6: Test specimens. (a) L-hooked bolt (FW1). (b) Crossing ALC panel connector (FW2).

(a) (b) (c) (d)

(e) (f) (g)

Figure 7: Assembling process. (a) Construction of the steel frame. (b) Welding steel angle on the beam. (c) Hole drilling on the ALC panel. (d) Panels were assembled orderly. (e) Bolts were connected to the connectors. (f) Filling special patchwork binder. (g) MTS device was connected to the column.

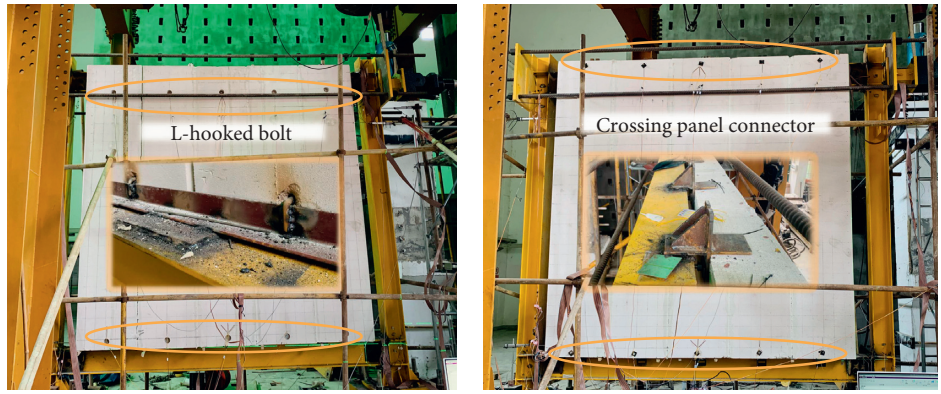

(a) (b)

Figure 8: Overview of the test specimens. (a) FW1. (b) FW2.

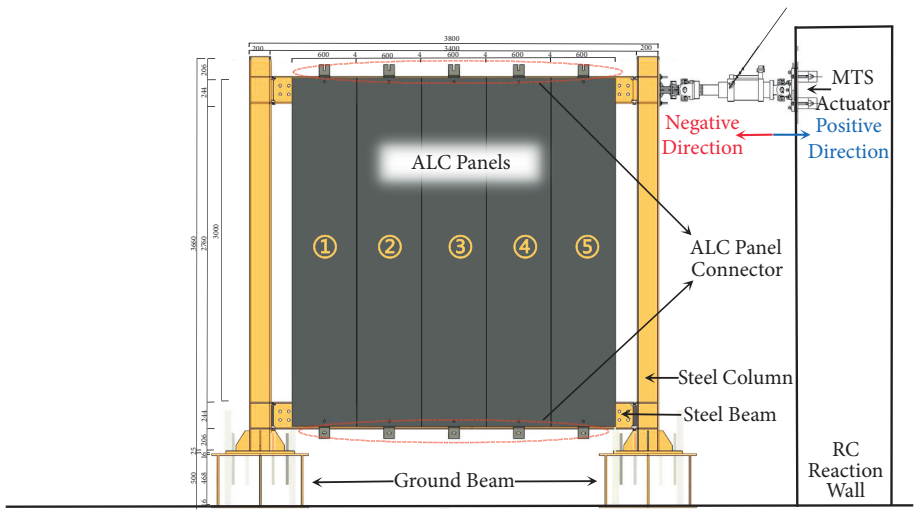

Figure 9: Schematic of test working conditions.

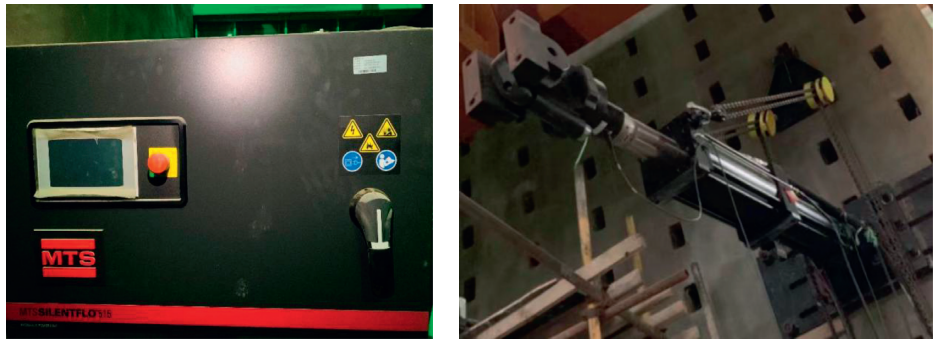

(a) (b)

Figure 10: Photograph of the test devices. (a) MTS servo loading system. (b) The actuator of MTS with the column.

Figure 11: Test ALC blocks and steel coupons.

The push-down is positive, whereas the pull-up is negative. Before 60 mm, displacement was applied three times for each displacement. After 60 mm, displacement was applied twice for each. This test was preloaded with 2 mm and loaded for three rotations to confirm that both the steel frame loading version and the booster's splice gap were properly adjusted [38]. The displacement load is identical to the size and material of the finite element analysis models described in Section 2, as shown in Figure 13.

4. Test Results

4.1. Specimen FW1. Specimen FW1 was a traditional L-hooked bolt used to rigidly connect the external ALC panel to the steel frame. When the displacement load reached the 6 mm stage, cracks in the joint mortar at the bottom of the No. 1 and No. 2 panel joints emerged. In the 10–12 mm stage, little chunks of ALC panels fell off continuously. When load achieved the 15 mm stage, there was

Figure 12: Universal testing machine.

Table 1: Material properties of steel.

Specimen		Sectional dimension (mm)	Thickness (mm)	Yield stress (MPa)	Ultimate stress (MPa)	Elongation stress (%)
Beam (HM)	Flange	$244 \times 175 \times 7 \times 11$	11	263.4	401.6	25.2
	Web		7	275.3	411.3	22.3
Column (HW)	Flange	$200 \times 200 \times 8 \times 12$	12	289.5	435.4	24.7
	Web		8	278.2	409.8	20.8
Connector	Q345	—	10	376.6	510.1	19.6

Table 2: Material properties of the ALC panel.

Specimen	Dimension (mm)	Measured compressive strength (MPa)	Elastic modulus (GPa)
Sac1	$100 \times 100 \times 100$	3.89	
Sac2	$100 \times 100 \times 100$	2.97	
Sac3	$100 \times 100 \times 100$	3.26	
Sac4	$100 \times 100 \times 100$	3.78	
Sac5	$100 \times 100 \times 100$	3.96	
Sac6	$100 \times 100 \times 100$	3.49	
Average		3.56	
Sae1	$100 \times 100 \times 300$		1640
Sae2	$100 \times 100 \times 300$		1880
Sae3	$100 \times 100 \times 300$		1790
Average			1770

visible dislocation between the panels which had fallen off the patchwork joints, as illustrated in Figure 14(a). Angle steel welds on the upper portion of the No. 2 panel failed when the displacement was in the 60 mm stage, as shown in Figure 14(b), and the L-hooked bolt hole started cracking. Therefore, when the displacement reached the 75 mm stage, the L-hooked bolt hole under the No. 3 panel developed a large crack. Besides, under No. 4 and No. 5 panels, the corners of each panel came away from the L-hooked bolt holes, revealing extensive fissures at bolt holes. Meanwhile, the holes of bolts began to expand, and the bolt swings with the steel angle as the displacement is applied as shown in Figures 14(c) and 14(d). When the displacement reached 90 mm, the welds of the left upper beam-column joints were fractured by loud sound, as shown in Figure 14(e). When it reached the 120 mm stage, the large areas of damage in the corners fell off, until it reached 135 mm, where several welds fractured as shown in Figure 14(f).

4.2. Specimen FW2. Specimen FW2 is the new connector (crossing ALC panel connector). When the displacement reached the 30 mm stage, the friction sound between the enclosure reinforcement and the end panel became audible. The frame and panel are unchanged, and only the bolts at the upper panel connector have dropped into their bolt holes,

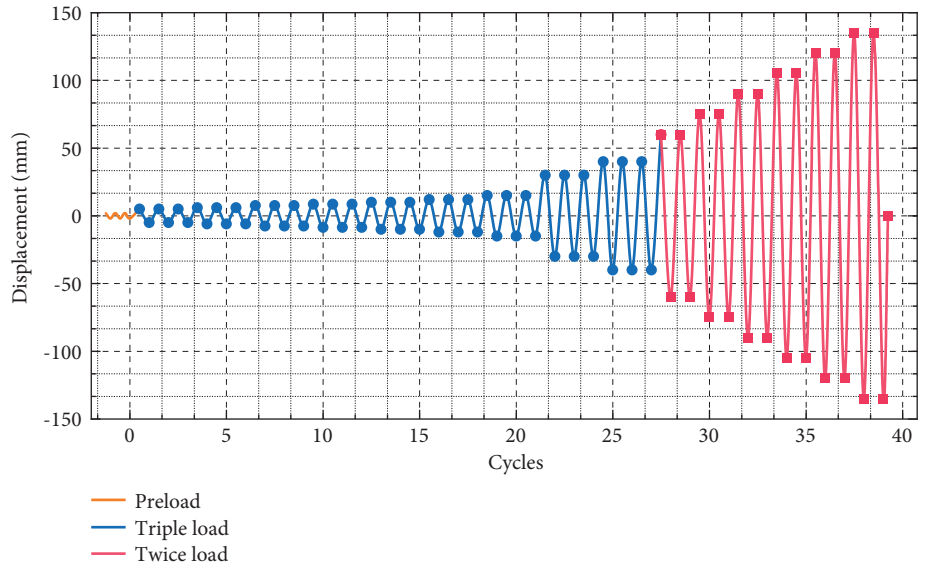

Figure 13: Loading system of the test.

Figure 14: Test results of FW1. (a) Obvious dislocation between panels. (b) Angle steel weld fractured. (c) Extended cracks at bolt holes. (d) The broken phenomenon of the panel angle. (e) Weld fractured. (f) Large areas of damage in each panel corner.

indicating that the junction follower performance is quite good, as illustrated in Figure 15(a). When arrived 40 mm, small pieces of debris came off, and the corner of the panel behind panel No. 5 was broken. When loading to 60 mm, the splicing mortar between No. 1 and No. 2 panels was broken, cracks appeared in the lower left panel corner of No. 1 panel, cracks appeared in the corner of No. 2 panel, and the relative movement between No. 1 and No. 2 panels could be seen. When loading to 75 mm, cracks appeared at the upper bolt holes of No. 2 and No. 3 panels, and the lower node of the second panel was loose, and obvious panel dislocation could be seen, as illustrated in Figure 15(b). When it arrived at 90 mm, the mortar of the joints collapsed in panels, and the corner of the back of the No. 1 panel was broken off, as shown in Figure 15(c). When loaded to 105 mm, the back corner of panel No. 3 was broken off, and the weld at the upper left beam-column node was chipped, as demonstrated in Figure 15(d). When loaded to the 120 mm stage, all the mortar of the joints of each panel was broken off, the weld at the upper left beam-column node was chipped, and the upper corner of panel No. 5 was broken off, as presented in Figure 15(e). When loaded to 135 mm, the back of panel No. 4 was diagonally cracked.

4.3. Load (Force)-Displacement Hysteretic Behavior. Figure 16 illustrates the cyclic response curves (hysteretic curves) obtained from the traditional L-hooked bolt and crossing panel connector (FW1 and FW2), respectively. As the displacement of the column end increases, the overall stiffness and strength of FW1 at the same amount of loading degrade, and the same process occurs in FW2, though to a lesser extent. This is primarily due to that the frame gradually transitions from the elastic to the elastic-plastic and plastic stages, as well as mortal splitting between ALC panels or blocks, cracking or crushing on the ALC panels' plastic deformation, and welding fracture at the beam-to-column and wall-to-frame connectors, all of which result in the destroying of the composite frame.

Two different types of ALC panel-connected frames have inverse S-shaped hysteresis curves. The area of FW2 is larger than that of FW1, which means the new connector has the better energy dissipation than the traditional L-hooked bolt. It further illustrates the excellent capacity of the new connector for steel frames. At the same late-stage displacement level, the new connector group (FW2) has a better bearing capacity than the L-hooked bolt group (FW1). Furthermore, specimen FW1 is shown to be more brittle than FW2 in terms of test phenomena and hysteretic behavior. This is because of the weld between the L-hooked bolt group (FW1) fractures at the 60–75 mm stage, resulting in a loss of stiffness and load-carrying ability after 75 mm, despite the fact that its load-carrying capacity is previously greater than that of the other groups. In comparison, FW2 absorbs energy during the early stage (before 30 mm) and provides the frame with increasing load capacity during the later stage due to the restricted displacement of the slip on the limitation hole.

5. Experimental Results' Analysis and Discussion

5.1. Skeleton Curves. Figure 17 shows the skeleton curves of the test connector specimens. The horizontal load-displacement skeleton curves for the tested specimens are produced by linking the maximum load point at each displacement level to the load-displacement hysteretic curves. Three stages of elasticity, elastomer-plasticity, and damage are observed on two specimens. The skeleton curves are approximately S-shaped, and the deterioration in stiffness is more apparent. The characteristic parameters of the skeleton curves are presented in Table 3, which indicates that the average of maximum force load-bearing capabilities in the positive and negative loading directions is 163.54 kN and 171.97 kN for FW1 and FW2, respectively. The maximum force load-bearing capacities of FW2 increase slightly by 5.2%, compared to FW1. However, it is much obvious in the positive loading direction (9.8% increasing). The calculation diagram of the yield point and the ultimate point is shown in Figure 18 in which they are determined by the Park method [41]. The yield load factor is 0.75, and these points can be determined according to the sequence of numbers shown in Figure 18 [34]. As for average of yield force bearing capability, FW2 (161.12 kN) is larger than FW1 (141.47 kN) by 13.9%. The average yield point delays hugely, 54.88 mm for FW1 to 69.98 mm for FW2 (27.5% delay).

At the early period (5 mm–40 mm stage), the tendency of the two skeleton curves is almost identical, with FW1 being larger than FW2, indicating that both specimens are in the elastic stage. However, because the bolt of FW2 connectors slipped into the limitation holes under loading, their load capacity and stiffness would be lower than the L-hooked bolt (FW1), indicating that the new connector (FW2) has great energy dissipation. The fact that the partial stiffness of the new connector (FW2) is only obtained during the intermediate stage of the test (40 mm–75 mm stage) indicated that the displacement of the new connector bolt at the limitation hole has reached its limitation. It is because the rigid connector of FW1 enters the yield stage first, and the rise in load-carrying capacity of FW1 becomes flat as FW2 exceeds the displacement loading. At this point, the new connector (FW2) begins to obtain more stiffness to the frame, hence increasing the frame's load capacity. Each specimen is in the yield stage during the 75 mm–90 mm stage. The curve of FW1 swings abruptly and then rapidly decreases which is significantly less than FW2. It is because the weld between the L-hooked bolt (FW1) and angle steel is broken at the 75 mm stage so that the FW1 connector type becomes much flexible, and the stiffness of frame contribution decreases rapidly. The bearing capacity of the L-hooked bolt reaches its maximum and enters the damage phase immediately, and the maximum value is obviously less than the scenario with FW2. Then, at the 105 mm–135 mm stage, the overall frame's load capacity decreases with the gradual increase of the load, so both skeleton curves of test groups decrease, in which FW1 declines more obviously.

Figure 15: Test results of FW2. (a) Upper connector slipped within the bolt hole. (b) Cracks appeared at the upper bolt holes. (c) Corner of the panel back was broken off. (d) Weld of the beam-column node was chipped. (e) Corner and all mortar of joints were broken.

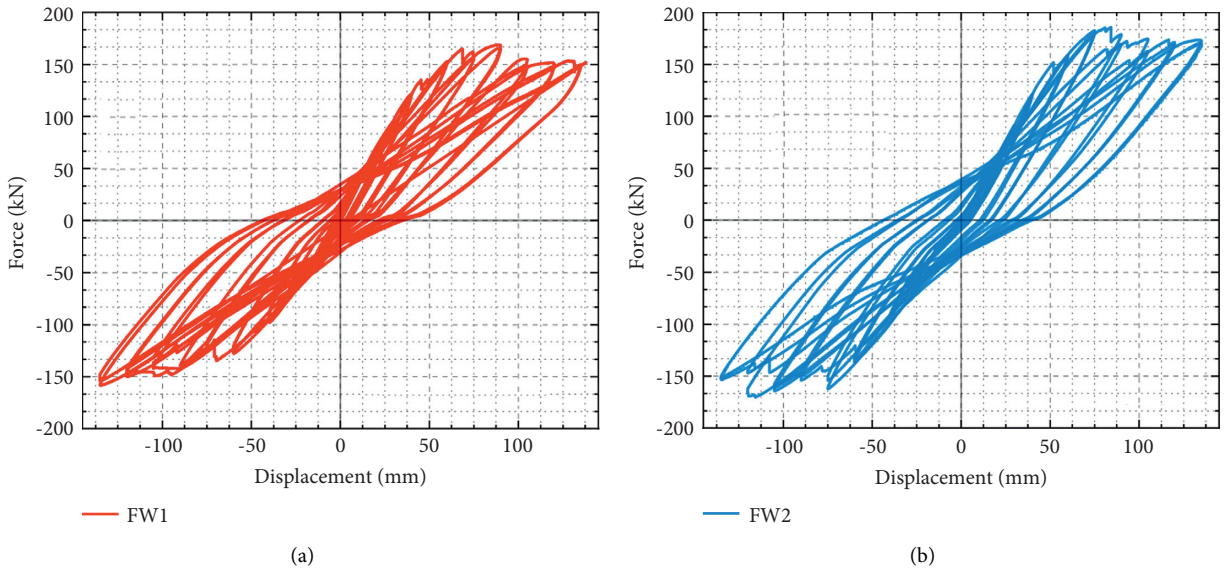

Figure 16: Load (force)-displacement hysteric curves of specimens. (a) Specimen FW1. (b) Specimen FW2.

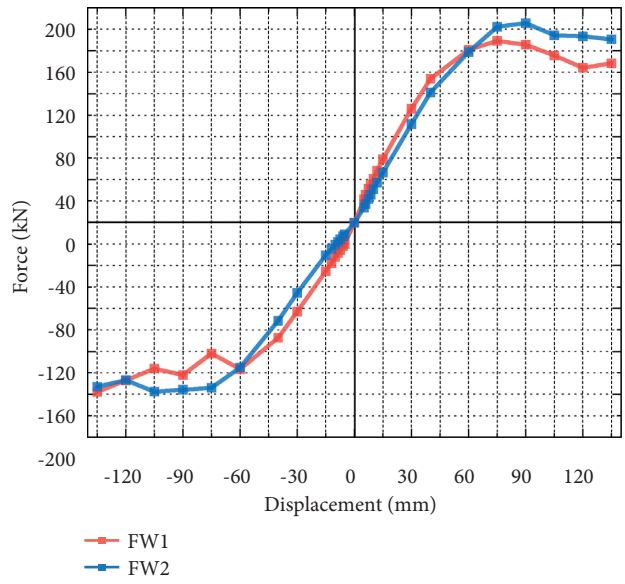

Figure 17: Skeleton curves of specimens FW1 and FW2.

Table 3: Skeleton curves of specimens.

Specimen	Direction	Yielding point		Peak point		Ultimate point	
		P_y (kN)	Δ_y (mm)	P_m (kN)	Δ_m (mm)	P_u (kN)	Δ_u (mm)
FW1	Push (+)	155.12	55.8	169.20	75.0	169.20	
	Pull (−)	127.82	54.0	157.89	135.0	121.85	
	Average	141.47	54.9	163.55	105.0	145.53	75.0
FW2	Push (+)	174.58	69.9	185.78	90.0	174.45	
	Pull (−)	147.74	70.1	158.15	105.0	157.64	
	Average	161.16	70.0	171.97	97.5	166.05	105.0

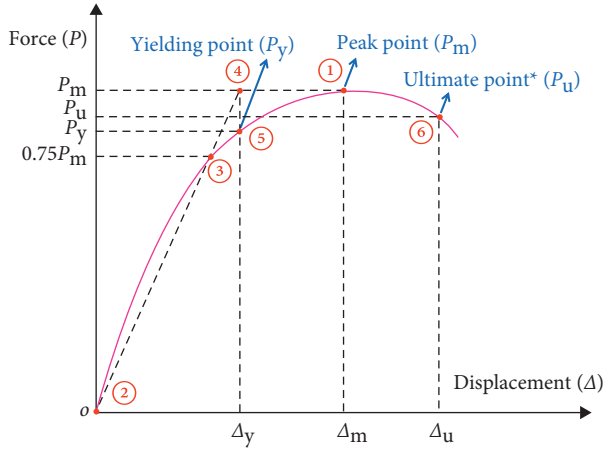

Figure 18: Schematic diagram of the method to determine characteristic points.

5.2. Ductility Coefficient. The high ductile structure has a high capacity for plastic deformation, which may prevent the emergence of brittle collapse and provide more time for people to try to hide or escape in the event of an earthquake or other accidents [42]. As a result, ductility is absolutely essential in seismic design. In this paper, Park's method is used to find the yield point in the skeleton curve. The ductility coefficient ($\mu = \Delta u/\Delta y$) of the test wall specimens in the positive and negative loading directions is shown in Table 4. The ductility is defined as the ratio of the ultimate displacement (Δu is the corresponding displacement when the lateral load value decreases to 85% of the load-bearing capacity or when the structural member is broken) to the yielding load displacement (Δy is the displacement when the structure first yields) on the ascending branch.

In Table 3, the 75 mm point is taken as the ultimate point of FW1 because the weld (between the L-hooked bolt and the angle steel) was fractured during the loading to ±75 mm stage. As for FW2, 105 mm is taken as the ultimate point because the new connector was fractured at the beam-column weld of the new connector during the ±105 mm stage. Each ductility coefficient of specimens in the positive and negative loading directions is calculated. It can be seen from the average values of specimens that the ductility coefficient of FW2 is larger than that of FW1 by 8.9%. It shows that the new connector has better ductility contribution to the structure.

5.3. Stiffness Degradation. The stiffness degradation factor of specimens versus displacement is described in Figure 19 to illustrate the stiffness deterioration. The stiffness degradation coefficient (K_j) is as follows [43]:

Table 4: Ductility coefficient of specimens.

Specimen	Push (+)	Pull (−)	Average
FW1	1.345	1.389	1.367
FW2	1.502	1.500	1.501

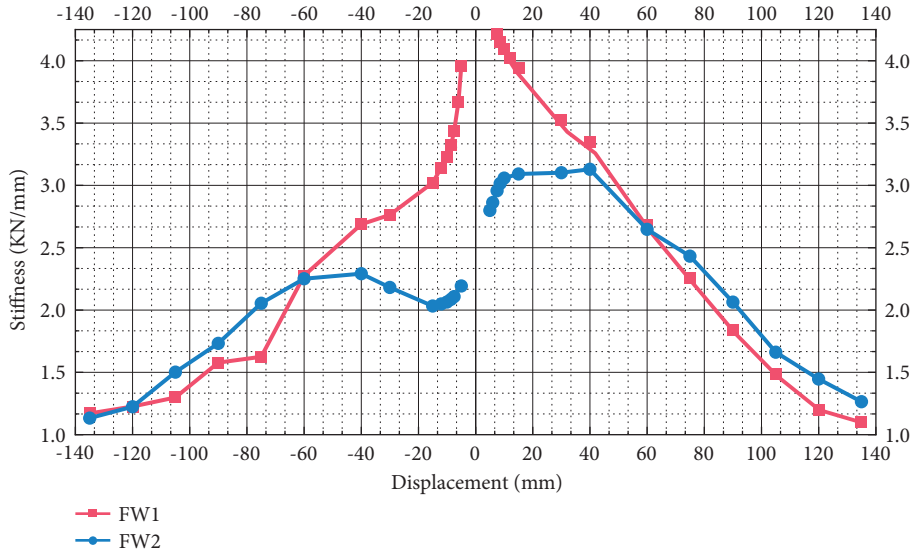

Figure 19: Comparing stiffness degradation of specimens FW1 and FW2.

$$K_j = \frac{\sum_{i=1}^{n} P_j^i}{\sum_{i=1}^{n} u_j^i}, \quad (1)$$

where P_j^i and u_j^i indicate the maximum load and displacement, respectively, during the ith loading cycle when the displacement equals j. The number of loading cycles in each loading cycle is defined by n.

As expected, stiffness of FW1 reduces significantly as lateral displacement increases. From the initial stiffness, it can be seen that FW1 (4.16 kN/mm average) is much larger than FW2 (2.50 kN/mm average) because the new joint is typically a flexible joint as its bolt swung in the limitation hole of the connector (which was consuming energy) during the early period. Therefore, the initial stiffness of FW2 is smaller, compared to the rigid joint of the traditional L-hooked bolt of FW1. In the 40 mm stage, the stiffness deterioration of FW2 appears to increase temporarily as the bolt of the new connector approached its limitation hole. Then, during 60–90 mm, the stiffness deterioration of FW1 falls significantly, while FW2 remains reasonably stable and exceeds FW1 at 60 mm, as illustrated in Figure 16. The averages of the two stiffness degradations following the elastic stage (75 mm) are 2.15 and 2.38, respectively, in which FW2 improves 10.6% compared to the traditional L-hooked bolt (FW1).

5.4. Energy Dissipation. The energy dissipation capacity of the structure in this test is measured by the area of force to displacement enclosed. The capacity of structural energy dissipation is directly proportional to the area of the hysteresis loop. The more the energy is dissipated by a structure, the safer and less is affected. The equivalent damping factor (ξ_e) was defined by the following equation [44]:

$$\xi_e = \frac{1}{2\pi} \cdot \frac{S_{ABC} + S_{CDA}}{S_{OBE} + S_{ODF}}, \quad (2)$$

where $S_{ABC} + S_{CDA}$ is the area enclosed by the hysteresis curve and $S_{OBE} + S_{ODF}$ is the sum of the areas of the two triangles, as shown in Figure 20.

The equivalent damping factor (ξ_e) versus the displacement relationship of specimens is shown in Figure 21. The trend of the FW1 curves is that ξ_e reduces rapidly during the 0–10 mm and then increases rapidly (after 10 mm). This indicates that the ALC panel is compressed by the L-hooked bolt, and the hole becomes larger. As for FW2, it raises quickly in the 0–40 mm stage because the bolts of the new connectors are dissipating energy by sliding in the limitation holes. Then, it declines slowly after 40 mm and raises after 60 mm rapidly because when the bolt reaches its limitation hole, the panels start to be compressed. At the displacement less than 60 mm, ξ_e of FW2 is larger than that of FW1. Subsequently, FW1 is slightly larger than FW2 because of the broken weld joints and the part of damage of the ALC panel. Then, it is overtaken by them after 80 mm because of the partial destruction of the ALC panel of FW2. However, FW2 is overtaken by FW1 at the 130 mm stage because almost every weld of FW1 is broken, making the connector completely flexible, while the new connector is working stably. The equivalent damping factor (ξ_e) of the new connector (FW2) is obviously larger than the L-hooked bolt one (FW1)

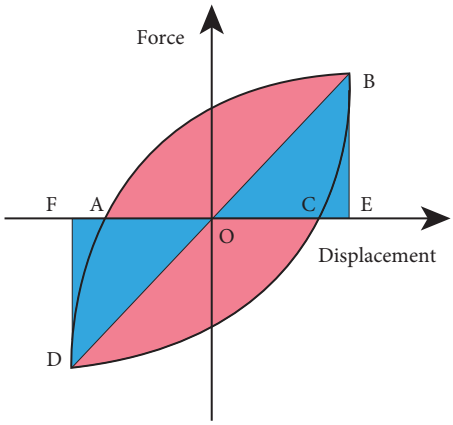

Figure 20: The dissipation capacity area.

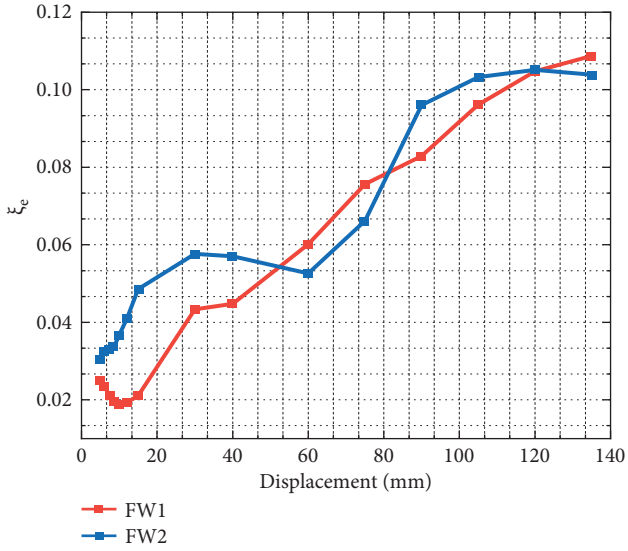

Figure 21: The equivalent damping factor (ξ_e) of specimens.

at the ultimate limit stage. At the yield state, the equivalent damping factor of FW2 increases by 10.2%, compared to FW1. As for the ultimate state, FW2 increases by 35.3%. The energy dissipation parameters of specimens at the yield and ultimate state are shown in Table 5. Generally, the frame with new connectors with the ALC panel has good dissipated energy capacity.

Table 5: Energy dissipation parameters of specimens at the yield and ultimate state.

Specimen	Yielding point		Ultimate point	
	Δ_y (mm)	$\xi_{e,y}$	Δ_u (mm)	$\xi_{e,u}$
FW1	54.88	0.05619	75	0.07564
FW2	69.98	0.06171	105	0.10232

5.5. Verification of Finite Element Results. The simulation results of ABAQUS are validated by comparing them to the test data, as shown in Figures 22–24. Specifically, the hysteresis curve and skeleton curve results indicate that the positive directions are nearly similar, the ABAQUS simulation trend is generally similar with the trend of the test, and the initial stiffness of the simulation results is slightly greater than that of the test results. Additionally, the test hysteresis curve's "pinch" effect is more significant than the simulation results. It is because the slipping of the ground beam occur during large displacement loading in test. The FEM simplifies the complex boundary conditions in the experiment (slippage of the ground beam, small gaps between specimens, etc.) [36]. Moreover, the steel mesh slippage on the ALC panel was not considered. However, all of the above differences are within a reasonable range [45]. As a result,

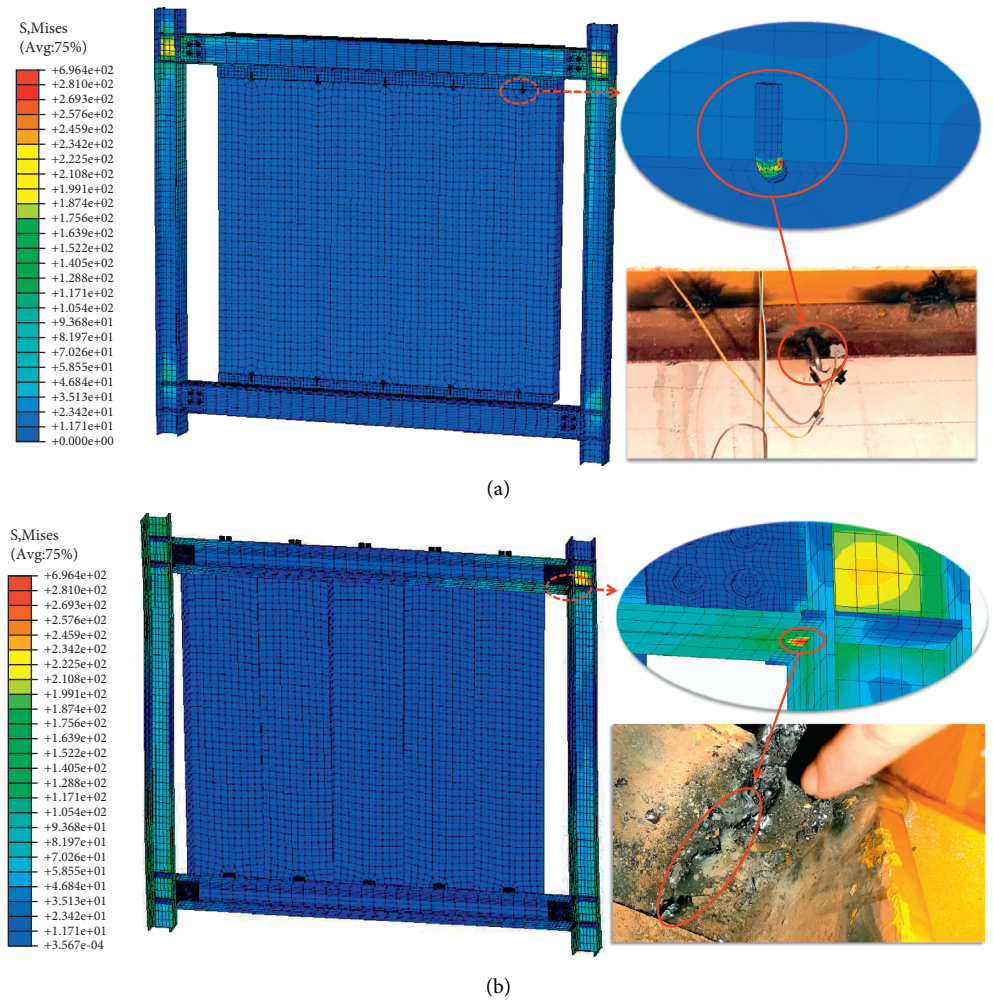

Figure 22: Comparing test observations and finite element simulation. (a) L-hooked bolt. (b) New crossing ALC panel.

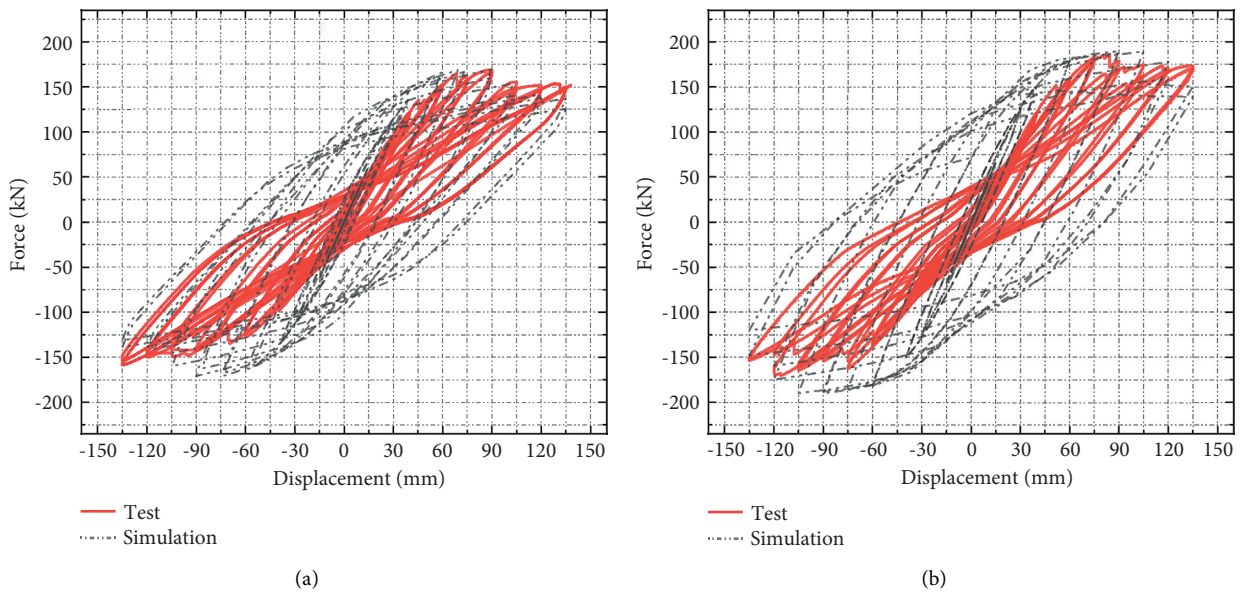

Figure 23: Comparing force-displacement hysteric of specimens in the test and simulation. (a) L-hooked bolt. (b) New crossing ALC panel.

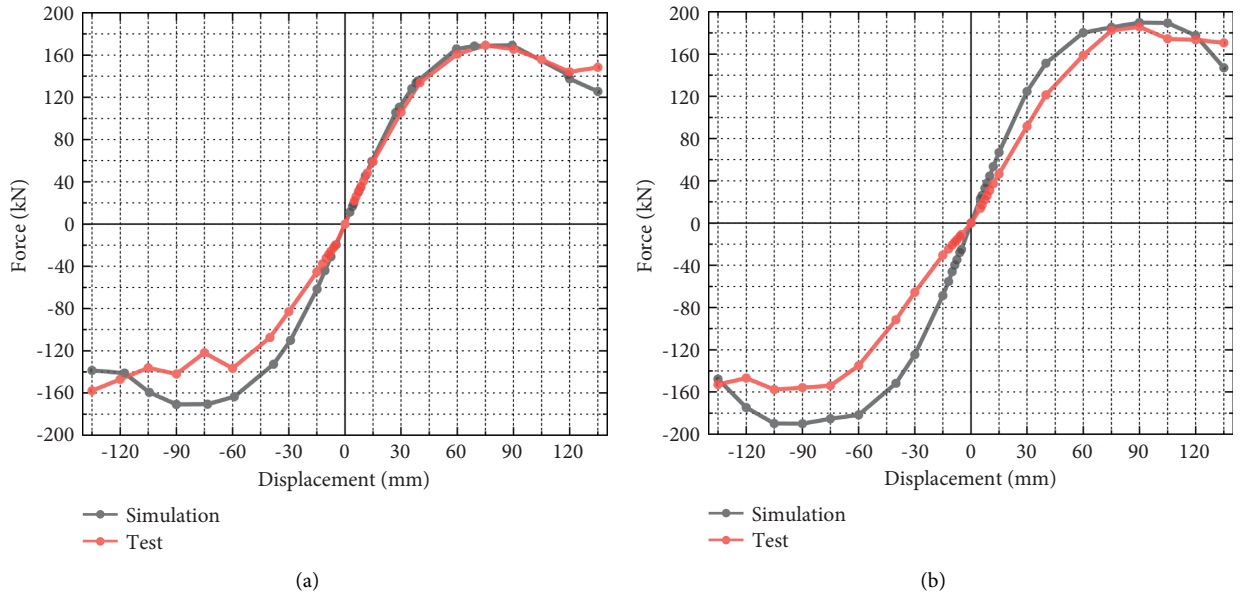

Figure 24: Comparing skeleton curves of specimens in the test and simulation. (a) L-hooked bolt. (b) New crossing ALC panel.

the finite element model and analysis method could accurately reflect the structure's seismic capacity of the new ALC panel connector and L-hooked bolt.

6. Conclusion

In this paper, a new flexible ALC panel connector is invented for solving construction problems. The FEMs were established, and the full-scale tests in low-cyclic loading were carried out. It has better seismic and synergistic capacities of panels, especially in the small earthquakes (cracks occur late). In the large earthquake, it can also provide certain stiffness to the structure. The new crossing connector has a wide range of applications, which can replace traditional connectors for steel buildings. The results are shown as follows:

(1) The new connector has better seismic capability. Its synergistic capacity is better as the occurrence of cracks in the wall of the ALC panel of the new connector is much later than the L-hooked bolt. By comparing the L-hooked bolt, the maximum bearing capability of the structure of the new connector increases by 5%, the yield bearing capability increases by 13.9%, and the yield displacement delays by 27.5%, resulting in the ductility increasing by 9.8%.

(2) The new connector worked stably in the full-scale low-cyclic loading test, while the weld of the traditional L-hooked bolt was fractured at the 75 mm stage. After the new connector reaches its limitation of the limitation hole, the maximum load capacity of the frame increases by 5.2% compared with the L-hooked bolt. The damage pattern is the same for both specimens. The joint of panels is the first to be damaged, followed by the hole and corner of the ALC panel.

(3) Although the L-hooked bolt has relatively larger initial stiffness, its stiffness degradation rate is larger than the new connector and decreases by 10.6% in the elastic stage, benefitting from the design of the limitation hole of the new flexible connector, which makes the structure's energy consumption capacity rise significantly. The equivalent damping factor of the new connector increases by 10.2% and 35.3% at the yield and ultimate state each.

(4) The result of the finite element simulation is similar with the test roughly, and the crossing connector has better seismic capability. The test hysteresis curve's "pinch" effect is more significant than the simulation results, which is in reasonable range. This finite element model by ABAQUS can simulate the new connector and L-hooked bolt in structures accurately, and the results of FEMs have reference value.

Data Availability

The data of the test and simulation used to support the findings of this study are included within the article.

Conflicts of Interest

The authors declare that they have no conflicts of interest.

Authors' Contributions

Kewei Ding conceptualized the study, provided resources, and edited and reviewed the article. Chikun Zhang provided the methodology, performed simulation , test, and analysis, wrote the original draft, and edited and reviewed the article. Shulin He performed simulation and test and edited the article. Yunlin Liu conceptualized the study and provided resources.

Acknowledgments

This research was financially supported by the National Natural Science Foundation of China (11472005), the University Synergy Innovation Program of Anhui Province (GXXT-2019-005), and the University-Industry Collaborative Education Program of the Ministry of Education (202002129042).

References

[1] Y. C. Kurama, S. Sritharan, and R. B. Fleischman, "Seismic-resistant precast concrete structures: state of the art," *Journal of Structural Engineering*, vol. 144, no. 4, Article ID 03118001, 2018.

[2] M. I. Khan, M. A. Al-Osta, S. Ahmad, and M. K. Rahman, "Seismic behavior of beam-column joints strengthened with ultra-high performance fiber reinforced concrete," *Composite Structures*, vol. 200, pp. 103–119, 2018.

[3] B. Cheng, K. Lu, J. Li, H. Chen, X. Luo, and M. Shafique, "Comprehensive assessment of embodied environmental impacts of buildings using normalized environmental impact factors," *Journal of Cleaner Production*, vol. 334, Article ID 130083, 2022.

[4] B. Li, "The present situation and development of prefabricated building in China," *China Science and Technology Information*, vol. 7, pp. 114-115, 2014.

[5] D. Zhang, G. Kuai, H. Xu, L. Luo, and H. Leng, "Application research of autoclaved sand aerated concrete wall panel in fabricated steel structure system," *Steel Structure*, vol. 31, no. 1, pp. 89–93, 2016.

[6] W. Li, X. Yang, Y. Wang, R. Shang, Y. Gui, and Z. Hou, "Application of composite insulation wall panel in a prefabricated steel structure building," *Industrial Building*, vol. 50, no. 3, pp. 147–150+123, 2020.

[7] J. J. Wang, J. H. Xie, J. H. He, M. Sun, J. Yang, and L. Li, "Combined use of silica fume and steel fibre to improve fracture properties of recycled aggregate concrete exposed to elevated temperature," *Journal of Material Cycles and Waste Management*, vol. 204, pp. 384–398, 2020.

[8] J. Wang and B. Li, "Cyclic testing of square CFST frames with ALC panel or block walls," *Journal of Constructional Steel Research*, vol. 130, pp. 264–279, 2017.

[9] A. Raj, D. Sathyan, and K. M. Mini, "Physical and functional characteristics of foam concrete: a review," *Construction and Building Materials*, vol. 221, pp. 787–799, 2019.

[10] R. Hay and C. P. Ostertag, "Life cycle assessment (LCA) of double-skin façade (DSF) system with fiber-reinforced concrete for sustainable and energy-efficient buildings in the tropics," *Building And Environment*, vol. 142, pp. 327–341, 2018.

[11] A. Artino, G. Evola, G. Margani, and E. M. Marino, "Seismic and energy retrofit of apartment buildings through autoclaved aerated concrete (AAC) blocks infill walls," *Sustainability*, vol. 11, no. 14, p. 3939, 2019.

[12] M. Kalpana and S. Mohith, "Study on autoclaved aerated concrete: review," *Materials Today Proceedings*, vol. 22, pp. 894–896, 2020.

[13] X. Qu, Z. Chen, and G. Sun, "Experimental and numerical analysis study on the structural performance of autoclaved aerated concrete (AAC) wall slab," *Journal of Building Materials*, vol. 15, no. 2, pp. 268–273, 2012.

[14] G. D. Matteis and R. Landolfo, "Diaphragm action of sandwich panels in pin-jointed steel structures: a seismic study," *Journal of Earthquake Engineering*, vol. 4, no. 3, pp. 251–275, 2000.

[15] Y. Yang, D. Zhang, P. Chen, and F. Gao, "Hysteretic capacity test of articulated steel frame with embedded ALCpanel," *Journal of Civil Engineering and Management*, vol. 38, no. 5, pp. 118–124, 2021.

[16] B. Wang, J. Wang, H. Wan, H. Hou, and J. Wang, "Research on capacity and connector structure of filling wall of high-rise steel structure building under cyclic loading," *Construction steel structure progress*, vol. 17, no. 6, pp. 44–50, 2015.

[17] G. Zhang, W. Xiao, B. Chen, Q. Miao, and H. Wu, "Research on hysteretic capacity of autoclaved aerated concrete external wall," *Industrial Building*, vol. 46, no. 11, pp. 86–92, 2016.

[18] L. Gou, F. Guo, Y. Yang, Z. Wang, and G. Zhu, "Installation technology of autoclaved lightweight Aerated concrete (ALC) wall panel in prefabricated steel frame structure," *TianJin Technology*, vol. 45, no. 11, pp. 56–59, 2018.

[19] T. S. Kim, H. Kuwamura, and T. J. Cho, "A parametric study on ultimate strength of single shear bolted connections with curling," *Thin-Walled Structures*, vol. 46, no. 1, pp. 38–53, 2008.

[20] K. Ding and W. Chen, "Experimental study and restoring force modeling on seismic capacity of prefabricated concrete beam-column joints," *Journal of Shenyang Jianzhu University (Natural Science)*, vol. 37, no. 1, pp. 51–60, 2021.

[21] J. Wu, J. Lu, Z. Xu, and Z. Zheng, "Upper load-bearing joint design method of the precast concrete wall panels," *Building Structure*, vol. 44, no. 13, pp. 47–51, 2014.

[22] F. Jin, A. Guo, and Z. Wang, "Application of autoclaved lightweight aerated concrete slab in internal partition and retaining wall," *Construction Technology*, vol. 30, no. 8, pp. 24-25, 2001.

[23] S. Dai, "Structural capacity and supporting Technology of steel frame-concrete tube housing," Doctoral dissertation, *Wuhan University of Technology*, Wuhan, China, 2004.

[24] L. Li and R. Chong, "20 years of work review of Nanjingxu Construction, a world-class ALC enterprise with craftsman spirit," in *Proceedings of the 35th Annual Meeting of China Aerated Concrete Association*, pp. 60–70, Weifang, Shandong, China, December 2015.

[25] S. Cao, G. Shu, K. Lin, S. Fan, and H. Gao, "Analysis and design method of a new type of prefabricated steel structure external wall panel joint," *Building Structure*, vol. 47, no. 10, pp. 46–52, 2017.

[26] X. Wang, X. Liu, L. Ma, and X. Zhou, "Experimental study on seismic capacity of assembled ALC external wall panel," *Steel Structure*, vol. 32, no. 4, pp. 22–26+63, 2017.

[27] Y. Meng, "Research on lateral force resistance of steel frame with multi-layer inner cladding wall panel," Doctoral dissertation, *Harbin Institute of Technology*, Harbin, China, 2012.

[28] L. Bai, "Development and mechanical properties study of the connector betweenALC wall panels and steel frame," Doctoral dissertation, *Shenyang Jianzhu University*, Shenyang, China, 2015.

[29] Y. Lin, K. Liu, T. Xiao, and C. Zhou, "Shear bearing capacity of framework joints of steel-reinforced concrete-filled circular steel tube," *Advances in Materials Science and Engineering*, vol. 2020, Article ID 7324865, 15 pages, 2020.

[30] Z. Chen, "Study on deformation behavior of steel frameexternal ALC wallboard under earthquake action," Doctoral dissertation, *Chongqing University*, Chongqing, China, 2017 .

[31] L. Huang, W. Lv, and Z. Yi, "Finite element analysis of a new composite wall-slab," *Journal of Central South University of Forestry & Technology*, vol. 3, pp. 54–58, 2002.

[32] Y. Zhou, T. Chen, Y. J. Pei, X. Hu, W. Yi, and L. Deng, "Static load test on progressive collapse resistance of fully assembled precast concrete frame structure," *Engineering Structures*, vol. 200, Article ID 109719, 2019.

[33] J. Wang, Q. Li, and G. Wei, "Seismic performance analysis of steel beam to CFST column connection with ductility and energy dissipation components," *Journal of Vibroengineering*, vol. 22, no. 1, pp. 131–144, 2020.

[34] E. Tuncer, B. Binici, and E. Canbay, "Behavior and design of FRP bonded autoclaved aerated concrete beams," *Construction and Building Materials*, vol. 282, Article ID 122712, 2021.

[35] C. Liu, J. Hou, Y. Hao, H. Hao, and X. Meng, "Effect of high strain rate and confinement on the compressive properties of autoclaved aerated concrete," *International Journal of Impact Engineering*, vol. 156, Article ID 103943, 2021.

[36] K. Ding, D. Zong, Y. Liu, and S. He, "Experimental and finite element analysis of external ALC panel steel frames with new semi-rigid connector," *Applied Sciences*, vol. 11, no. 22, Article ID 10990, 2021.

[37] D. Zhao, L. Chen, and W. Wang, "Hysteretic behavior analysis of Steel frame structure with ALC walls," *Journal of Zhejiang University of Technology*, vol. 38, no. 4, pp. 448–452, 2010.

[38] K. Ding, Y. Ye, and W. Ma, "Seismic performance of precast concrete beam-column joint based on the bolt connection," *Engineering Structures*, vol. 232, Article ID 111884, 2021.

[39] H. Lu, H. Zhang, K. Ma, Q. Wu, and L. Jiang, "Experimental study and numerical study on shear bearing capacity of shear key joints of reinforced concrete open-web sandwich plates," *Advances in Materials Science and Engineering*, vol. 2021, Article ID 6197472, 22 pages, 2021.

[40] D. Wang, H. Zhao, and X. Lv, "Loading protocols for quasi-static test of structural components for buildings," *Sichuan Building Science*, vol. 40, no. 3, pp. 62–67, 2014.

[41] R. Park and T. Paulay, *Reinforced Concrete Structures*, Willey, New York, NY, USA, 1975.

[42] J. Xu, J. Wang, H. S. Mohamed et al., "Post-earthquake fire resistance of bolted end-plate connection joint with end-plate and web stiffeners," *Journal of Constructional Steel Research*, vol. 185, Article ID 106835, 2021.

[43] K. Ding and Y. Zhang, "Experimental study on seismic performance of fabricated bolted joint under low-cycle reciprocating loads," *Results in Engineering*, vol. 9, Article ID 100208, 2021.

[44] Y. Ma and J. Jia, "The influence of different parameter on the seismic behavior of SRUHSC frame," *Advances in Materials Science and Engineering*, vol. 2017, Article ID 3495150, 2017.

[45] W. Ma, K. Xu, and B. Cheng, "Experimental study on the seismic behavior of a new single-faced superposed shear wall with the concealed column," *Structures*, vol. 33, pp. 4446–4460, 2021.